



HAL
open science

Modeling and control of a decoupled hybrid-fed Multi-Active Bridge (MAB) converter

Rebecca Tarraf, Baptiste Morel, David Frey, Sylvain Leirens, Sébastien Carcouet, Xavier Maynard, Yves Lembeye

► **To cite this version:**

Rebecca Tarraf, Baptiste Morel, David Frey, Sylvain Leirens, Sébastien Carcouet, et al.. Modeling and control of a decoupled hybrid-fed Multi-Active Bridge (MAB) converter. PCIM Europe 2023, May 2023, Nüremberg, Germany. pp.1750-1758, 10.30420/566091242 . cea-04208958

HAL Id: cea-04208958

<https://cea.hal.science/cea-04208958v1>

Submitted on 15 Sep 2023

HAL is a multi-disciplinary open access archive for the deposit and dissemination of scientific research documents, whether they are published or not. The documents may come from teaching and research institutions in France or abroad, or from public or private research centers.

L'archive ouverte pluridisciplinaire **HAL**, est destinée au dépôt et à la diffusion de documents scientifiques de niveau recherche, publiés ou non, émanant des établissements d'enseignement et de recherche français ou étrangers, des laboratoires publics ou privés.

Modeling and Control of a Decoupled Hybrid-Fed Multi-Active Bridge (MAB) Converter

Rebecca Tarraf¹, Baptiste Morel¹, David Frey², Sylvain Leirens¹, Sébastien Carcouet¹, Xavier Maynard¹, Yves Lembeye²

¹ Université Grenoble Alpes, CEA, Leti, F-38000 Grenoble, France

² Université Grenoble Alpes, G2Elab, CNRS, F-38000 Grenoble, France

Corresponding author: Rebecca Tarraf, rebecca.tarraf@cea.fr

Abstract

Multi-Active Bridge (MAB) converters are the extension of the well-known Dual-Active Bridge (DAB) bidirectional DC-DC converter. This multiport structure has attracted a lot of attention recently, especially for applications soliciting renewable energy sources and energy storage systems. Generally, MAB structures are based on voltage converters. However, in some cases, it could be interesting to have a current-fed input port due to load characteristics or operation constraints. This leads to a hybrid MAB structure mixing both current-fed and voltage-fed bridges. In the first part of this paper, the operation of a current-fed DAB converter topology is investigated. Additionally, a continuous-time model is developed for this topology and a control strategy is proposed. In the second part, the elaborated work is generalized to a decoupled hybrid-fed MAB converter. Simulation results using Matlab/Simulink are presented to validate this study.

1 Introduction

The integration of renewable energy sources and energy storage systems in modern power electronics applications drew greater attention to multiport converters in recent years. These structures form an Energy Hub where the production, consumption and storage of electrical energy can be done in one place [1]. Multi-Active Bridge (MAB) converters are multiport converters provided with intrinsic galvanic isolation. This is due to the connection of this topology's ports through a high frequency (HF) transformer. Galvanic isolation is crucial for applications where different energy sources/loads with important voltage dissimilarities should be connected together.

Current-fed DAB converters present several advantages compared to a classical voltage-fed DAB converter such as soft switching on the full operation range and the absence of an input capacitor at the current-fed port. This can be interesting for different applications like connecting a PV panel or a battery system to the current-fed port [2]–[5]. Some previous works addressed different topologies of multiport hybrid-fed converters [6]–[8]. In this paper, a new topology of a fully isolated, decoupled hybrid-fed MAB converter was studied, modelled and controlled.

In the first part of this paper, the continuous-time model of a current-fed DAB converter is developed. The mathematical modeling of a system helps with the study of its dynamic behavior and controller design. The main drawback that the current-fed port introduces into the system is the complexity of its control. In fact, the current inverter will impose control restrictions on all the other ports of the system. The non-compliance of these restrictions may cause brutal over-voltages that could destroy the circuit. A control method is proposed in this paper, based on the elaborated mathematical model and the control constraints. The second part of this paper extends this work for a decoupled, hybrid-fed MAB converter, having any number of ports. Simulation results are displayed to validate the developed model and control strategy.

2 Current-Fed DAB Converter

2.1 Topology and Working Concept

Figure 1 shows the studied topology of a current-fed DAB converter connected to a current source at its primary port and a voltage source at its secondary port.

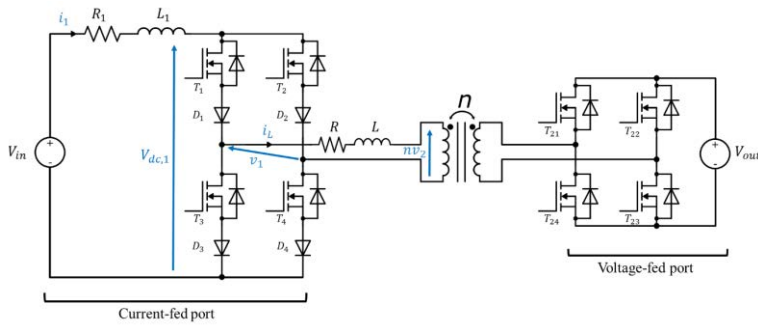


Fig. 1 Current-fed Dual-Active Bridge (DAB) converter topology.

The waveforms of this DAB's AC signals circulating in the transformer are shown in Fig. 2, all along with the command signals of switches T_1 of the current inverter and T_{21} of the H-Bridge. These shapes are an approximation of the real signals' shapes. In reality, the current i_L is not perfectly trapezoidal, as it is slightly affected by the switching of the secondary H-bridge at instants t_1 and t_4 .

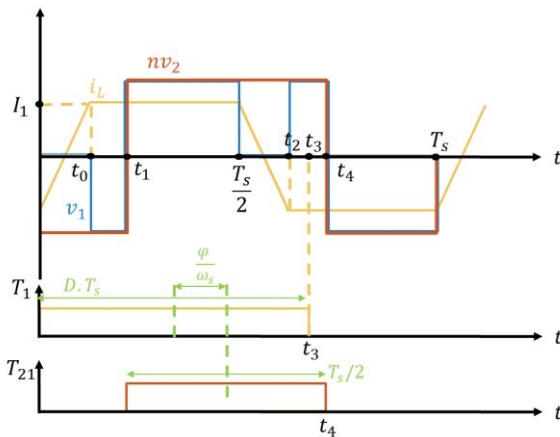


Fig. 2 AC signals at the DAB converter's transformer with the command signals of switches T_1 and T_{21} .

As shown in Fig. 2, D is the command duty cycle of switch T_1 , with $D > 0.5$, and φ is the phase shift angle in radians between the commands of T_1 and T_{21} . T_s is the switching period (f_s is the switching frequency). The command duty cycle of the secondary H-Bridge switches is fixed to 50% on all the operation range, so v_2 is a 2-level voltage as shown in Fig. 2.

The operation cycle of this current-fed DAB converter is divided into the following time intervals:

- $0 \leq t \leq t_0$:

At $t = 0$, switches T_1 and T_4 are turned on. T_2 and T_3 were already ON right before $t = 0$ from the previous cycle. Since all the current i_1 was passing through T_2 and T_3 , the switching of T_1 and T_4 is done at zero current (ZCS), thus decreasing the switching losses. In this time interval, all the current inverter's switches are ON, so the voltage

$v_1 = 0$ (Fig. 3.a). On the voltage port, the AC voltage should be $v_2 = -V_{out} < 0$ in order to reverse the transformer current, so T_{22} and T_{24} are ON. Therefore, the transformer current increases from $-I_1$ to I_1 in this interval and is represented by the following expression (neglecting the value of the transformer's series resistance R):

$$i_L(t) = -\frac{nv_2}{L}t - I_1 = \frac{nV_{out}}{L}t - I_1 \quad (1)$$

Where n is the turn ratio of the transformer and L is the link inductance between the ports. I_1 is the value of the input current at a certain operating point. This current is considered constant at each operating point as it is limited by the input inductance L_1 , which's value is a lot bigger than the value of the link inductance L .

As i_L gets closer to I_1 , the current starts passing more through diodes D_1 and D_4 and less through D_2 and D_3 . At $t = t_0$, D_2 and D_3 are naturally turned off.

- $t_0 \leq t \leq \frac{T_s}{2}$:

In this time interval, the input current passes through T_1 , T_4 , D_1 and D_4 and $i_L = I_1$ (Fig. 3.b). Switches T_2 and T_3 are turned off between t_0 and t_1 at zero current (ZCS) since D_2 and D_3 are blocking the current. At $t = t_1$, the voltage port's H-Bridge is switched at zero voltage (ZVS) since $i_L > 0$ (T_{22} and T_{24} are turned off while T_{21} and T_{23} are turned on). Therefore, $v_2 = V_{out} > 0$ (Fig. 3.c). Ideally, the switching of the voltage port does not affect the transformer's current value since it is imposed by the current source ($L_1 \gg L$). However, it will allow the transformer current to reverse again in the next time interval.

- $\frac{T_s}{2} \leq t \leq t_2$:

At $t = T_s/2$, T_2 and T_3 are turned on at zero current. Therefore, all the current inverter's switches are ON again and the voltage $v_1 = 0$ (Fig. 3.d). The transformer current decreases from I_1 to $-I_1$ since $nv_2 > 0$ in this interval and it is represented by the following expression:

$$i_L(t) = -\frac{nv_2}{L}\left(t - \frac{T_s}{2}\right) + I_1 = -\frac{nV_{out}}{L}\left(t - \frac{T_s}{2}\right) + I_1 \quad (2)$$

At $t = t_2$, D_1 and D_4 are naturally blocked.

- $t_2 \leq t \leq T_s$:

The input current passes entirely through T_2 , T_3 , D_2 and D_3 in this time interval and $i_L = -I_1$. At $t = t_3$, T_1 and T_4 are turned off at zero current. At $t = t_4$, the voltage port's H-bridge is switched with ZVS and $v_2 = -V_{out} < 0$. This cycle is then repeated for each switching period T_s .

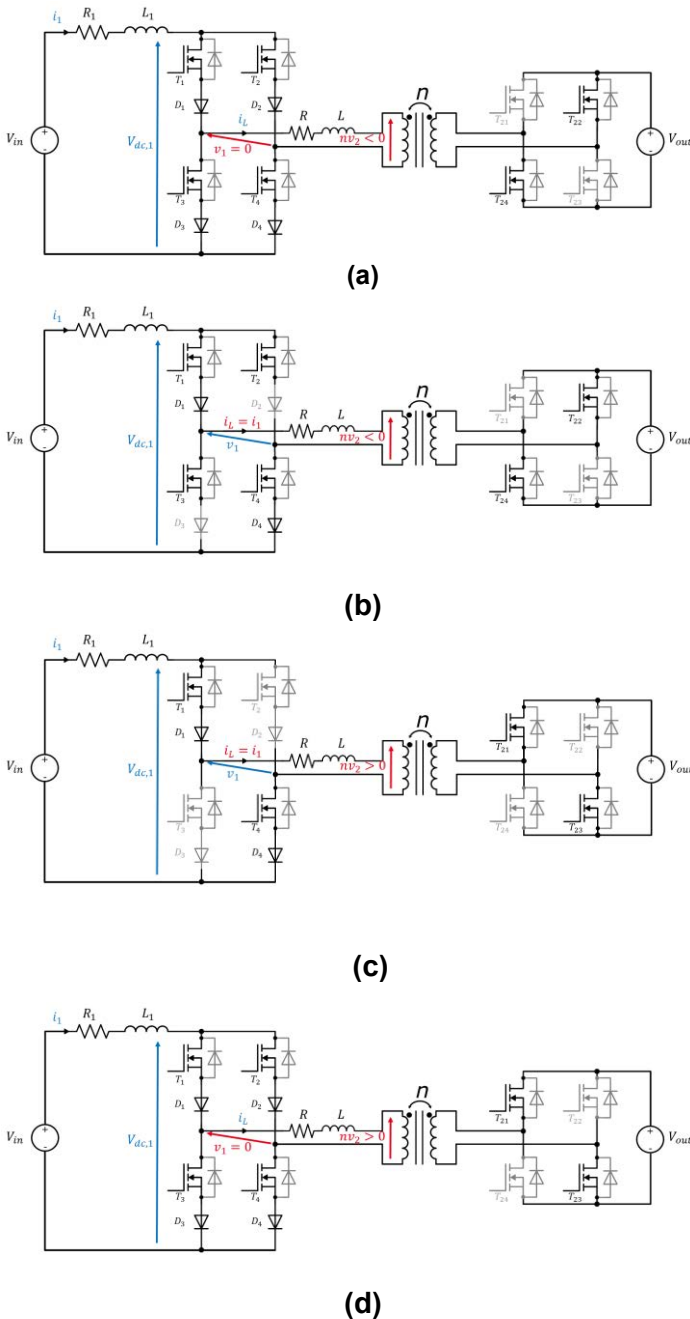


Fig. 3 Equivalent circuits of the DAB converter at: (a) $0 < t < t_0$ (b) $t_0 < t < t_1$ (c) $t_1 < t < T_s/2$ (d) $T_s/2 < t < t_2$.

2.2 Operating Conditions

In order to be able to transfer power from port 1 to port 2 with soft switching on the whole operation range at both active bridges, while avoiding over-voltages at port 1, two main conditions should be respected:

- a) In order to avoid over-voltages and to have a soft switching at the primary side, the switches of the current inverter should not be turned off before the complete reversal of the transformer current and the blocking of their series

diodes. Otherwise, these switches would block an important current in the link inductance, which will cause brutal over-voltages at the current port. This means that:

$$t_3 \geq t_2 \rightarrow DT_s \geq \frac{T_s}{2} + t_0$$

With $t_0 = \frac{2LI_1}{nV_{out}}$ from eq. (1).

Therefore,

$$D \geq \frac{2LI_1}{nV_{out}T_s} + \frac{1}{2} \quad (3)$$

- b) The voltage port's AC voltage v_2 should be reversed after the transformer current's full reversal and the blocking of both the diodes and their series switches. If v_2 is reversed before that, over-voltages will occur at the primary side. Additionally, the current might not be able to reverse, so no power would be exchanged between the two ports. If v_2 is reversed before the blocking of the primary's switches ($t_2 < t_4 < t_3$), the diodes could be turned on again. This condition also ensures a soft switching at the voltage port and it can be written as :

$$t_4 \geq t_3 \rightarrow \frac{DT_s}{2} + \varphi \frac{T_s}{2\pi} + \frac{T_s}{4} \geq DT_s$$

Therefore,

$$D \leq \frac{\varphi}{\pi} + \frac{1}{2} \quad (4)$$

As we can notice, these conditions depend on the operating point of the converter as I_1 , D and φ vary according to the desired input power. This is what makes the control of this topology of a current-fed DAB converter more complex than a DAB converter with 2 H-bridges.

2.3 Mathematical Modelling of the Current-Fed DAB Converter

In general, the mathematical model of a system makes the study of its dynamic behavior easier, giving valuable information about its response characteristics such as stability margins and time response. Additionally, it helps with the design of its controllers. For the proposed current-fed DAB converter, the state space equations are:

- $L_1 \frac{di_1}{dt} = V_{in} - V_{dc,1} - R_1 \cdot i_1$
- $L \frac{di_L}{dt} = v_1 - nv_2 - R \cdot i_L$

We can also write, from Fig. 1 and Fig. 2:

$$V_{dc,1} = \begin{cases} v_1 & \text{for } 0 \leq t \leq \frac{T_s}{2} \\ -v_1 & \text{for } \frac{T_s}{2} \leq t \leq T_s \end{cases}$$

By considering the transformer current perfectly trapezoidal, and by neglecting the transformer resistance R , we can write :

$$V_{dc,1} = \begin{cases} 0 & \text{for } 0 \leq t \leq t_0 \\ -nV_{out} & \text{for } t_0 \leq t \leq t_1 \\ nV_{out} & \text{for } t_1 \leq t \leq \frac{T_s}{2} \end{cases}$$

Therefore, $V_{dc,1}$ has a period of $T_s/2$ and can be written as $V_{dc,1} = S_0 \cdot nV_{out}$ with:

$$S_0 = \begin{cases} 0 & \text{for } 0 \leq t \leq t_0 \\ -1 & \text{for } t_0 \leq t \leq t_1 \\ 1 & \text{for } t_1 \leq t \leq \frac{T_s}{2} \end{cases}$$

The first state equation becomes:

$$L_1 \frac{di_1}{dt} = V_{in} - S_0 \cdot nV_{out} - R_1 \cdot i_1 \quad (5)$$

The state variable i_1 of Eq. (5) is DC. Therefore, in order to have a continuous-time model, i_1 can be represented by its average value, which is the 0th coefficient of its Fourier series representation.

Considering that $\langle x \rangle_k(t)$ is the k^{th} coefficient of the Fourier series of a variable x , we can write:

$$L_1 \frac{d\langle i_1 \rangle_0}{dt} = \langle V_{in} \rangle_0 - n\langle S_0 \rangle_0 \langle V_{out} \rangle_0 - R_1 \langle i_1 \rangle_0 \quad (6)$$

With:

$$\langle S_0 \rangle_0 = \frac{2}{T_s} \int_0^{\frac{T_s}{2}} S_0(t) \cdot dt = \frac{2}{T_s} \left(t_0 + \frac{T_s}{2} - 2t_1 \right),$$

where:

$$t_0 = \frac{2L\langle i_1 \rangle_0}{nV_{out}} \quad (\text{from Eq. (1)})$$

$$t_1 = \frac{DT_s}{2} + \varphi \frac{T_s}{2\pi} - \frac{T_s}{4} \quad (\text{from Fig. 2})$$

Therefore:

$$\langle S_0 \rangle_0 = \frac{4L}{nV_{out}T_s} \langle i_1 \rangle_0 + 2 - 2D - 2\frac{\varphi}{\pi} \quad (7)$$

Equation (6) becomes:

$$L_1 \frac{d\langle i_1 \rangle_0}{dt} = - \left(R_1 + \frac{4L}{T_s} \right) \cdot \langle i_1 \rangle_0 + \langle V_{in} \rangle_0 - 2 \cdot \left(1 - D - \frac{\varphi}{\pi} \right) \cdot n\langle V_{out} \rangle_0 \quad (8)$$

The approximations that were done made the first equation of the state space representation enough to get the relation between current I_1 (the control output) and the control parameters φ and D .

The small-signal model of this system is obtained by linearizing it about an operating point and then applying a perturbation to its variables. The variables will therefore be represented as:

$$\langle x \rangle = x_{eq} + \widehat{x}$$

Where variables with the symbol “ $\widehat{}$ ” represent the small signals (perturbations around the operating point) and x_{eq} represents the value of $\langle x \rangle$ at the operating point, also called equilibrium point.

The linearization of Eq. (8) around an operating point is done using Taylor series expansion. The variations of the input and output voltages around their average values can be neglected ($\langle \widehat{V_{in}} \rangle_0 = \langle \widehat{V_{out}} \rangle_0 = 0$) since their dynamics are considered relatively slow. Therefore, we can write:

$$L_1 \frac{d\widehat{\langle i_1 \rangle_0}}{dt} = - \left(R_1 + \frac{4L}{T_s} \right) \cdot \widehat{\langle i_1 \rangle_0} + \frac{2nV_{out}}{\pi} \cdot \widehat{\varphi} + 2nV_{out} \cdot \widehat{D} \quad (9)$$

At the equilibrium point, where all the dynamics are zero ($\frac{d\widehat{\langle i_1 \rangle_0}}{dt} = 0$), we can write:

$$I_{1,eq} = \left(V_{in} - 2nV_{out} \cdot \left(1 - D_{eq} - \frac{\varphi_{eq}}{\pi} \right) \right) \times \frac{1}{R_1 + \frac{4L}{T_s}} \quad (10)$$

2.4 Control of the Input Current

From Eq. (10), we can notice that, at a certain operating point, the input current I_1 depends on the command duty cycle D and the phase shift φ . An infinity of combinations of the values of D_{eq} and φ_{eq} can give us the same desired input current value $I_{1,eq}$, as long as conditions of Eq. (3) and Eq. (4) are respected.

We can get the expression of φ_{eq} in function of D_{eq} and $I_{1,eq}$ from Eq. (10) as follows:

$$\varphi_{eq} = \pi \cdot \left(\frac{R_1 I_{1,eq}}{2nV_{out}} + \frac{2L I_{1,eq}}{nV_{out} T_s} - \frac{V_{in}}{2nV_{out}} - D_{eq} + 1 \right)$$

By choosing the value of D_{eq} to be equal to its minimum allowed value expressed in Eq. (3), with a certain added safety margin ϵ , we get:

$$D_{eq} = D_{min} + \epsilon = \frac{2L I_1}{nV_{out} T_s} + \frac{1}{2} + \epsilon.$$

Therefore,

$$\begin{aligned} \varphi_{eq} &= \pi \cdot \left(\frac{R_1 I_{1,eq}}{2nV_{out}} - \frac{V_{in}}{2nV_{out}} + \frac{1}{2} - \epsilon \right) \\ &\approx \pi \cdot \left(\frac{1}{2} - \frac{V_{in}}{2nV_{out}} - \epsilon \right) \end{aligned} \quad (11)$$

R_1 has a relatively small value compared to other terms of this equation, so it can be neglected. We notice from Eq. (11) that for $D_{eq} = D_{min} + \epsilon$, the phase shift φ_{eq} does not depend on the operating point anymore. Therefore, to move from a certain operating point to another (in order to change the input current's desired value), we do not need to modify the value of φ (as long as the input and output voltages are constant). Only the modification of the duty cycle D is required, making it easier for conditions of Eq. (3) and Eq. (4) to be respected.

The maximum allowed value D_{max} of D , given in Eq. (4), also becomes independent of the operating point since it is a function of φ . From Eq. (3), Eq. (10) and Eq. (11), we can get the corresponding maximum reachable value of the input current:

$$I_{1,max} = \frac{nV_{out} - V_{in}}{\frac{4L}{T_s} - R_1} \quad (12)$$

The approximations that were done in the developed mathematical model will lead to a steady state error if only an open loop (a feedforward) control is applied. A feedback with a PI controller is therefore added in order to cancel this error.

The closed-loop control block diagram of the input current I_1 is shown in Fig. 4. A safety margin $\epsilon = 0.01$ for the control of D was taken into consideration ($D_{eq} = D_{min} + \epsilon$). This value was chosen arbitrarily in this study. In future works, a more accurate margin value could be calculated by taking into consideration the variations of the voltage sources, the error on the values of the inductances, current and voltage sensors, etc...

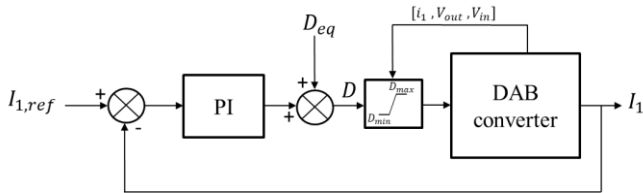


Fig. 4 Block diagram of the input current closed-loop control of the current-fed DAB converter.

The open loop transfer function of this control loop can be calculated from the Laplace transform of Eq. (9) and has the following expression:

$$G_{i1}(s) = \left. \frac{\hat{I}_1(s)}{\hat{D}(s)} \right|_{\varphi=0} = \frac{\frac{2nV_{out}}{L_1}}{s + \left(\frac{R_1}{L_1} + \frac{4L}{L_1 T_s} \right)} = \frac{g}{\tau s + 1} \quad (13)$$

It is a first order transfer function with a gain g and a time constant τ .

The PI controller's transfer function is:

$$C(s) = \frac{K \cdot (T_i \cdot s + 1)}{T_i \cdot s}$$

We choose $T_i = \tau$. The closed loop transfer function will therefore become:

$$CLTF(s) = \frac{C(s)G_{i1}(s)}{1 + C(s)G_{i1}(s)} = \frac{1}{\frac{\tau}{K \cdot g} \cdot s + 1}$$

Consequently, the new time constant would be:

$$\tau_a = \frac{\tau}{K \cdot g}$$

Knowing that the feedback time response to get to 95% of the desired input current value is $t_{r,95\%} = 3 \cdot \tau_a$, the gain K is chosen for a desired value of $t_{r,95\%}$, such that:

$$K = \frac{3 \cdot \tau}{t_{r,95\%} \cdot g}$$

3 Decoupled Hybrid-Fed MAB Converter

In this section, a TAB converter having two voltage-fed ports and one current-fed port is modelled and controlled (Fig. 5). The proposed TAB converter's ports are decoupled using the hardware decoupling technique described in [9]. Therefore, this converter will have a master port and two slave ports. The decoupling is ensured by having a low leakage inductance at the master port and relatively higher leakage inductances (with externally added series inductances) at the slave ports. Ideally, this will make the link inductance between the two slaves big enough so no (or little) power is directly exchanged between them. The link inductance between a port #i and a port #j is calculated from the delta equivalent representation of the system as follows:

$$L_{ij} = \begin{cases} NA, & \forall i = j \\ L'_i + L'_j + L'_i L'_j \left(\sum_{k \neq i,j}^n \frac{1}{L'_k} \right), & \forall i \neq j \end{cases} \quad (14)$$

Where L'_i is the leakage inductance of port #i referred to a chosen reference side of the transformer which is port 1 in this work.

In this study, the master port will be port 2, which is a voltage-fed port. Ports 1 and 3 will be slave ports with port 1 being a current-fed port and port 3 a voltage-fed port, as shown in Fig. 5. The master port should be connected to a stiff voltage source such as the grid or a battery system [9]. Port 1 necessarily generates power so it can represent a PV panel for example, port 2 is bidirectional and port 3 is connected to a load.

Consequently, with $L_2 \approx 0$, we will have:

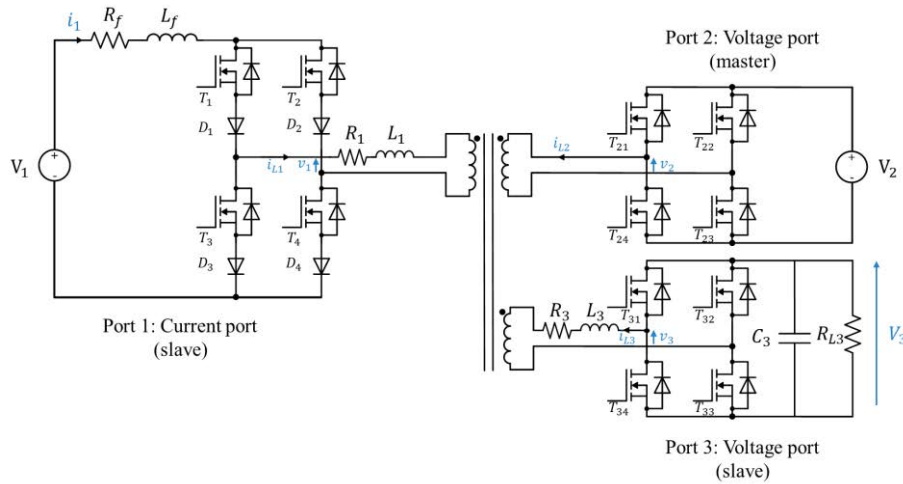


Fig. 5 Decoupled hybrid-fed Triple-Active Bridge (TAB) converter.

$$\begin{cases} L_{12} \approx L_1 \\ L_{23} \approx L_3' \\ L_{13} \approx \infty \end{cases}$$

Controlling the power flows of this converter can be done by regulating port 1's input current i_1 and port 3's output voltage V_3 .

3.1 Mathematical Modelling of the Decoupled Hybrid-Fed TAB Converter

By decoupling the ports of this TAB converter, this Multiple-Input Multiple-Output (MIMO) system is transformed into two independent Single-Input Single-Output (SISO) systems that can be modelled as two DAB converters. Ports 1 and 2 form the first SISO system which is a current-fed DAB converter having the topology described in the previous section. Ports 2 and 3 form the second SISO system, which is a classical DAB converter having two voltage-fed ports.

The modeling of the first SISO system was described in the first section. Therefore, by analogy, we can directly write the following transfer function for the control of the input current I_1 of port 1:

$$G_{i1}(s) = \left. \frac{\widehat{I}_1(s)}{\widehat{D}_1(s)} \right|_{\widehat{\varphi}_2=0} = \frac{\frac{2 \frac{n_1}{n_2} V_2}{L_f}}{s + \left(\frac{R_f}{L_f} + \frac{4L_1}{L_f T_s} \right)} \quad (15)$$

D_1 is the command duty cycle of port 1's switches and the control parameter of the input current I_1 .

$$G_{v3}(s) = \left. \frac{\widehat{V}_3(s)}{\widehat{d}_{23}(s)} \right|_{\widehat{v}_2=0}$$

$$= \frac{\frac{4b}{\pi C_3} \left(s + \frac{R_3}{L_3} - \frac{a}{b} w_s \right)}{s^3 + \left(2 \frac{R_3}{L_3} + \frac{1}{R_{L3} C_3} \right) \cdot s^2 + \left(\frac{R_3^2}{L_3^2} + w_s^2 + 2 \frac{R_3}{R_{L3} C_3 L_3} + \frac{8}{\pi^2 C_3 L_3} \right) \cdot s + \left(\frac{8R_3}{\pi^2 C_3 L_3^2} + \frac{R_3^2}{R_{L3} C_3 L_3^2} + \frac{w_s^2}{R_{L3} C_3} \right)}$$

n_1/n_2 is the turn ratio of the transformer between ports 1 and 2. The other parameters are represented in Fig. 5.

The same control conditions explained in the previous section apply for ports 1 and 2 of the decoupled hybrid-fed TAB converter. Accordingly, we can write:

$$D_1 \geq \frac{2L_1 I_1}{nV_2 T_s} + \frac{1}{2} \quad (16)$$

$$D_1 \leq \frac{\varphi_2}{\pi} + \frac{1}{2} \quad (17)$$

The mathematical modelling of the second SISO system, which is the classical voltage-fed DAB converter consisting of ports 2 and 3, can be found in many previous works [10], [11]. The generalized average model is used to accurately represent the AC signals of this system. The phase shift φ_{23} between the command signals of ports 2 and 3 is the control input parameter of the DC voltage V_3 of port 3. Equation (18) (shown in the bottom of this page) is the transfer function linking φ_{23} to V_3 in the frequency domain, where:

$$a = \frac{2}{L_3} \cdot \frac{n_3}{n_2} \cdot V_2 \cdot \cos(d_{23,eq} \pi)$$

$$b = -\frac{2}{L_3} \cdot \frac{n_3}{n_2} \cdot V_2 \cdot \sin(d_{23,eq} \pi)$$

with: $d_{23} = \frac{\varphi_{23}}{\pi}$.

3.2 Control Strategy

Port 1 is chosen to be the phase shift reference port of this system, so $\varphi_1 = 0$.

The first SISO system, which is equivalent to a current-fed DAB converter, is controlled as it was described in Section 2.4. Therefore, the command duty cycle D_1 of port 1 is set equal to its minimum allowed value expressed in Eq. (16), with an added safety margin ϵ . The command phase shift φ_2 of port 2 would therefore be fixed to the value given in Eq. (19) (as long as the voltage sources V_1 and V_2 are not perturbed), independently of the chosen operating point (i.e. the values of I_1 and V_3).

$$\varphi_{2,eq} = \pi \cdot \left(\frac{1}{2} - \frac{V_1}{2 \cdot \frac{n_1}{n_2} \cdot V_2} - \epsilon \right) \quad (19)$$

The phase shift φ_{23} between the command signals of ports 2 and 3 is calculated from the well-known power flow expression of a voltage-fed DAB converter, for a desired value of V_3 :

$$P_{23} = \frac{n_3 V_2 V_{3,eq}}{2 n_2 f_s L_{23}} \cdot \frac{\varphi_{23,eq}}{\pi} \cdot \left(1 - \frac{\varphi_{23,eq}}{\pi} \right),$$

where P_{23} is the power received by port 2 from port 3.

The steady state errors of the input current control of port 1 and the output voltage control of port 3 are cancelled by using PI controllers. The parameters of these PI controllers are calculated based on the transfer functions of Eq. (15) and Eq. (18) and the imposed response characteristics (e.g. time response, stability margins ...). The control block diagrams are presented in Fig. 6.

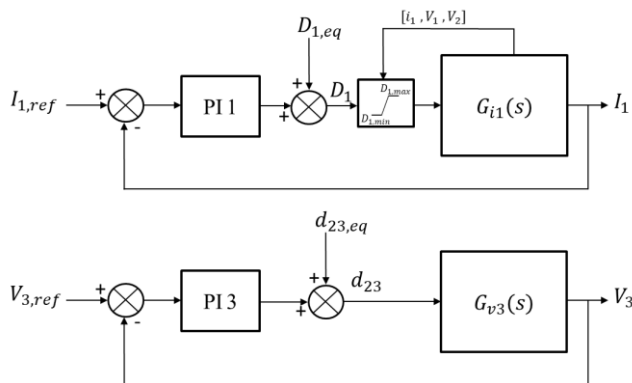


Fig. 6 Control block diagrams of the decoupled hybrid-fed TAB converter.

3.3 Simulation Results

The simulation platform that was used to validate this study is Matlab/Simulink.

The parameter values of the simulated decoupled hybrid-fed TAB converter are shown in Table 1.

Table 1 Parameter values of the decoupled hybrid-fed TAB converter.

Parameter symbol	Parameter value
V_1	200 V
V_2	400 V
R_{L3}	120 Ω
f_s	20 KHz
L_f	0.016 H
R_f	10 m Ω
L_1	83 μ H
R_1	10 m Ω
L_3	230 μ H
R_3	10 m Ω
C_3	100 μ H
R_{C3}	1 m Ω
L_m	8.3 mH
n_1	100 turns
n_2	83 turns
n_3	124 turns
P_{max}^*	4 KW

*maximum power exchanged between 2 ports

The simulation results of the decoupled hybrid-fed TAB converter are shown in Fig. 7.

Figure 7.a shows the response of the input current control of port 1 when a change of setpoint is introduced around its operating point. The chosen time response to get the parameter values of the loop's PI controller is $t_{r1,95\%} = 6ms$. We can see from Fig. 7.a that the simulated closed-loop time response is equal to its chosen value (6ms), which validates the developed mathematical model and control strategy.

Similarly, Figure 7.b shows the response of the output voltage control of port 3 when a setpoint change is applied to it around a certain operating point. The chosen time response for this loop is $t_{r2,95\%} = 60ms$ with an overshoot of 5%. These values are found in the response of the simulated model, thus validating this study.

Figure 7.c shows the AC voltages of the transformer windings at ports 1 and 2 with the AC current of port 1. The simulated waveforms match the theoretical ones in Fig. 2.

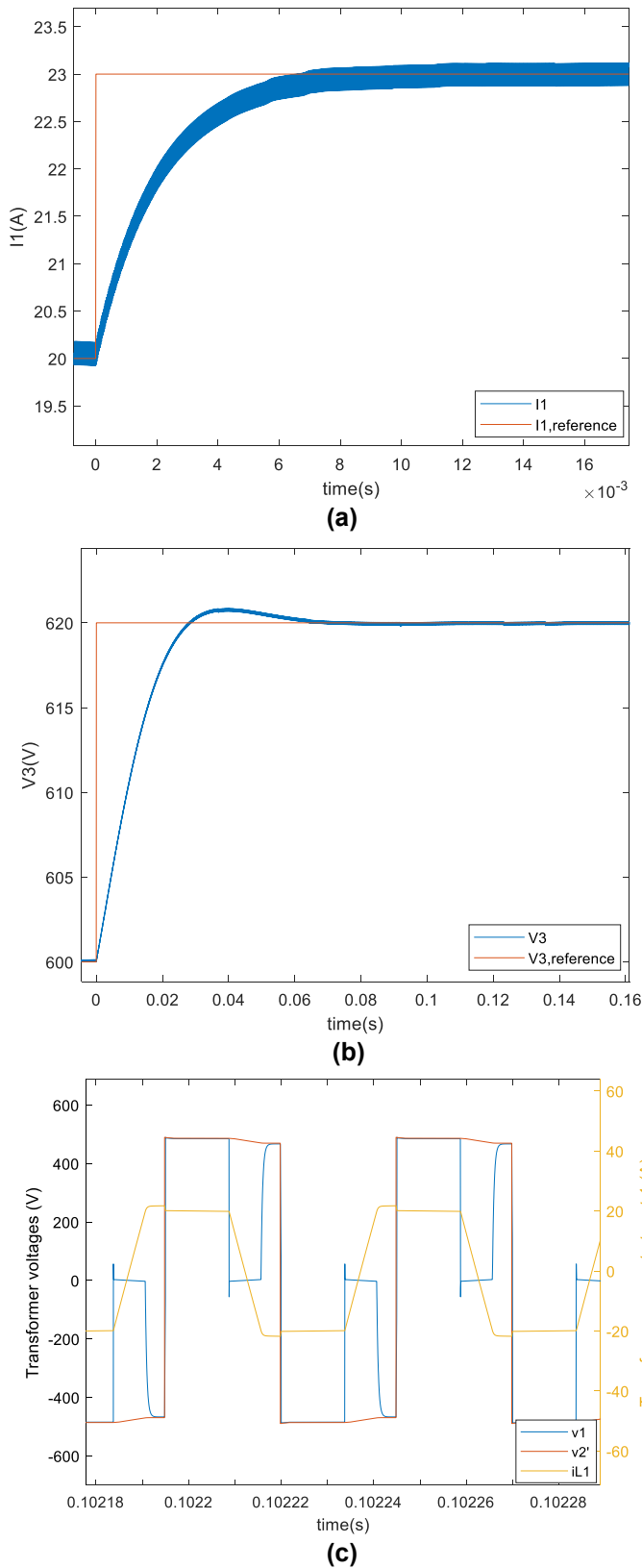


Fig. 7 Simulation results of the control loops developed for the decoupled hybrid-fed TAB converter: (a) input current control of slave current port 1 (b) output voltage control of slave voltage port 3 (c) transformer AC voltages of ports 1 and 2 and AC current of port 1 at the chosen operating point.

4 Conclusion

A hybrid-fed MAB converter is an interesting topology for many applications such as PV panels and battery storage systems. This is mainly due to their soft-switching performances on the whole operation range. In the first part of this paper, the mathematical modelling and control of a current-fed DAB converter topology were developed. The working concept of this topology was explained and so were the control conditions that should be respected for a safe functioning without over-voltages and with soft switching. This work was then extended in the second part for a decoupled hybrid-fed TAB converter. The mathematical model and the proposed control strategy were tested and validated using Matlab/Simulink.

The work presented in this paper can be generalized for a decoupled hybrid-fed MAB converter having a total of n ports, with m current-fed ports and $(n - m)$ voltage-fed ports. The master port should be a voltage-fed port connected to a stiff voltage source. The decoupling of this system allows the addition of as many ports as needed without increasing the complexity of its control.

In future works, a coupled hybrid-fed TAB converter having leakage inductances at all its ports will be investigated. The control restrictions will be reevaluated in order to elaborate a new mathematical model and control strategy for the coupled system.

5 References

- [1] M. Mohammadi, Y. Noorollahi, B. Mohammadi-ivatloo, and H. Yousefi, "Energy hub: From a model to a concept – A review," *Renewable and Sustainable Energy Reviews*, vol. 80, pp. 1512–1527, Dec. 2017, doi: 10.1016/j.rser.2017.07.030.
- [2] A. Blinov, D. Vinnikov, and V. Ivakhno, "Full soft-switching high step-up DC-DC converter for photovoltaic applications," in *2014 16th European Conference on Power Electronics and Applications*, Lappeenranta, Finland, Aug. 2014, pp. 1–7. doi: 10.1109/EPE.2014.6911013.
- [3] Z. Guo, K. Sun, T.-F. Wu, and C. Li, "An Improved Modulation Scheme of Current-Fed Bidirectional DC-DC Converters For Loss Reduction," *IEEE Trans. Power Electron.*, vol. 33, no. 5, pp. 4441–4457, May 2018, doi: 10.1109/TPEL.2017.2719722.
- [4] A. Chub, J. Rabkowski, A. Blinov, and D. Vinnikov, "Study on power losses of the full soft-switching current-fed DC/DC converter with

- Si and GaN devices,” in *IECON 2015 - 41st Annual Conference of the IEEE Industrial Electronics Society*, Yokohama, Nov. 2015, pp. 000013–000018. doi: 10.1109/IECON.2015.7392957.
- [5] A. Chub, R. Kosenko, and A. Blinov, “Zero-voltage switching galvanically isolated current-fed full-bridge DC-DC converter,” in *2016 10th International Conference on Compatibility, Power Electronics and Power Engineering (CPE-POWERENG)*, Bydgoszcz, Poland, Jun. 2016, pp. 455–459. doi: 10.1109/CPE.2016.7544231.
- [6] S. Kurm and V. Agarwal, “Current Fed Dual Active Bridge based Multi-Port DC/AC Converter for Standalone Solar PV fed Systems with Battery Backup,” in *2020 IEEE International Conference on Power Electronics, Drives and Energy Systems (PEDES)*, Jaipur, India, Dec. 2020, pp. 1–6. doi: 10.1109/PEDES49360.2020.9379447.
- [7] V. Rathore, K. Rajashekara, A. Ray, L. A. G. Rodriguez, and J. Mueller, “A Current-fed High Gain Multilevel DC-DC Converter for BESS Grid Integration Applications,” in *2021 IEEE Applied Power Electronics Conference and Exposition (APEC)*, Phoenix, AZ, USA, Jun. 2021, pp. 1964–1970. doi: 10.1109/APEC42165.2021.9487339.
- [8] D. Liu, “Topology, Development, and Control of a Three-Port Triple-Half-Bridge DC-DC Converter for Hybrid Energy Storage Application”.
- [9] S. Bandyopadhyay, P. Purgat, Z. Qin, and P. Bauer, “A Multiactive Bridge Converter With Inherently Decoupled Power Flows,” *IEEE Trans. Power Electron.*, vol. 36, no. 2, pp. 2231–2245, Feb. 2021, doi: 10.1109/TPEL.2020.3006266.
- [10] Hengsi Qin and J. W. Kimball, “Generalized Average Modeling of Dual Active Bridge DC–DC Converter,” *IEEE Trans. Power Electron.*, vol. 27, no. 4, pp. 2078–2084, Apr. 2012, doi: 10.1109/TPEL.2011.2165734.
- [11] P. Costa, P. Lobler, L. Roggia, and L. Schuch, “Modeling and Control of DAB Converter Applied to Batteries Charging,” *IEEE Trans. Energy Convers.*, vol. 37, no. 1, pp. 175–184, Mar. 2022, doi: 10.1109/TEC.2021.3082468.